



Republic of Iraq
Ministry of Higher Education
and Scientific Research
University of Diyala
College of Science
Department of Physics



Preparation and Characterization of Magnetic Ferrofluid MnZn Ferrite Nanoparticles

A Thesis

Submitted to the Council of the College of Science- University of Diyala in a
Partial Fulfillment of the Requirements for the Degree of Doctor of Philosophy
of Science in Physics

By

Hussein Sliman Mahmood

B.Sc. in Physics (2007)

M.Sc. in Physics (2017)

Supervised By

Prof. Dr.

Tahseen H. Mubarak

Prof. Dr.

Sabah M. Ali Ridha

2021 A

سُورَةُ طٰهٍ

بِسْمِ اللَّهِ الرَّحْمَنِ الرَّحِيمِ

فَتَعَلَى اللَّهِ الْمَلِكُ الْحَقُّ وَلَا تَعْجَلْ بِالْقُرْآنِ مِنْ قَبْلِ أَنْ
يُنزَلَ إِلَيْكَ وَحْيُهُ وَقُلْ رَبِّ زِدْنِي عِلْمًا ﴿١١٤﴾

صدق الله العلي العظيم

Dedication

My PhD thesis is dedicated to ...

My deceased father

**My supporters; mother, brothers, sisters and my
wife D,**

My beloved country Iraq

**The martyrs of Iraq with all the love and
appreciation**



Hussein. S. M.

Acknowledgement

First and foremost, I would like to thank Almighty Allah for giving me the strength, knowledge, ability and opportunity to undertake, persevere and complete this research. Without his blessings, this achievement would not have been possible.

There are many people I need to thank for their support and encouragement.

I would like to express my heartfelt thanks to my supervisors, **Prof. Dr. Tahseen H. Mubarak and Prof. Dr. Sabah M. Ali Ridha**, for their guidance, inspiration, and encouragement. I am very grateful for both their expertise and commitments throughout the course of my research.

I express my thanks to all members of Physics Department, especially postgraduate faculty members and staffs of the college for their cooperation.

My sincere thanks are to **Majeed Hameed Mustafa** an electrical engineer in Kirkuk Gas Power Plant, for help and support to design induction heater system.

I would also like to thank **Mr. Ihab Mohamed** for his help in making measurements in the Tehran university; Iran.

I offer my special thanks to my research colleagues and friends **Mr. Adnan, Mr. Mohamed Ihsan , Mr. Mohamed Nayf, Mr. Raad Kasym and Ms Shyma Mufeed** for their cooperation during the period of studies and thesis work.

Supervisors Certification

We certify that this thesis entitled "*Preparation and Characterization of Magnetic Ferrofluid MnZn Ferrite Nanoparticles* " for the student (**Hussein Sliman Mahmood**), was prepared under our supervisions at the Department of Physics, College of Science, University of Diyala in partial fulfillment of requirements needed to award the degree of *Doctor of Philosophy (Ph.D.) of Science in Physics*.

Signature: 

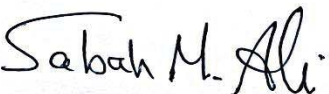
Name: **Dr. Tahseen H. Mubarak**

Title: Professor

Address: College of Science

University of Diyala

Date: 15/3 / 2021

Signature: 

Name: **Dr. Sabah M. Ali Ridha**

Title: Professor

Address: College of Education for

Pure Science

University of Kirkuk

Date: 15/3 / 2021

Head of the Physics Department

In view of available recommendation, I forward this thesis for debate by the examining committee.

Signature: 

Name: **Dr. Ammar A. Habeeb**

Title: *Asst. Professor*

Head of the Physics Department

Address: College of Science, University of Diyala

Date: 15/3 / 2021

Scientific Amendment

I certify that the thesis entitled "**Preparation and Characterization of Magnetic Ferrofluid MnZn Ferrite Nanoparticles**" presented by student (**Hussein Sliman Mahmood**) has been evaluated scientifically, therefore, it is suitable for debate by examining committee.

Signature



Name: Dr. Nidhal Nissan Jandow

Title: Professor

Address: Department of Physics / College of Education/ Mustansiriyah
University

Date: 20 / 4 / 2021

Scientific Amendment

I certify that the thesis entitled "**Preparation and Characterization of Magnetic Ferrofluid MnZn Ferrite Nanoparticles**" presented by student (**Hussein Sliman Mahmood**) has been evaluated scientifically, therefore, it is suitable for debate by examining committee.

Signature 

Name: Dr. Mukhlis M. Ismail

Title: Professor

Address: University of Technology / Applied Science Department

Date: 25 / 4 / 2021

Linguistic Amendment

I certify that the thesis entitled "*Preparation and Characterization of Magnetic Ferrofluid MnZn Ferrite Nanoparticles*" presented by (**Hussein Sliman Mahmood**) has been corrected linguistically; therefore, it is suitable for debate by examining committee.

Signature



Name: Dr. Esam Hamid Hameed

Title: Assistant Professor

Address: Department of Biotechnology, University of Diyala

Date: 18/4 /2021

Examination Committee Certificate

We certify that we have read this thesis entitled "*Preparation and Characterization of Magnetic Ferrofluid MnZn Ferrite Nanoparticles*" and, as an examining committee, we examined the student (**Hussein Sliman Mahmood**) on its content, and in what is related to it, and that in our opinion it meets the standard of a thesis for the degree of *Doctor of Philosophy of Science in Physics*.

(Chairman)


Signature 

Name: Dr. Nabeel A. BaKer

Title: Professor

Data: 14/6/2021

(Member)


Signature 

Name: Dr. Mahdi H. Suhail

Title: Professor

Data: 14/6/2021

(Member)

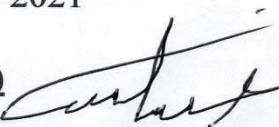
Signature 

Name: Dr. Shihab A. Zaidan

Title: Professor

Data: 14/6/2021

(Member)

Signature 

Name: Dr. Adnan Raad Ahmed

Title: Professor

Data: 14/6/2021

(Member)

Signature 

Name: Dr. Muhammad Hameed Al-TIMIMI

Title: Assistant Professor

Data: 13/6/2021

(Member /Supervisor)

Signature 

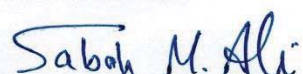
Name: **Dr. Tahseen H. Mubarak**

Title: Professor

Data: 14/6/2021

Signature

(Member /Supervisor)

Signature 

Name: **Dr. Sabah M. Ali Ridha**

Title: Professor

Data: 14/6/2021

Signature

Approved by the Council of the College of Science

(The Dean)

Signature: 

Date: 14/6/2021

Name: **Dr. Tahseen H. Mubarak**

Title: Professor

Abstract

Nanoparticles of $Mn_{1-x}Zn_xFe_2O_4$ have been prepared by co-precipitation method and followed by heat treatment in hydrothermal autoclave reactor; where x varied from 0 to 0.5, with amount of change 0.1 in every experiment. XRD results showed that it was difficult to prepare MnZn-ferrite directly by using the coprecipitation method. Field emission scanning electron microscopes (FESEM) images confirmed that the preparation method produced spherical nanoparticles with a slight change in the particle size distribution. The particle size has shrunk after the heat treatment. The average particle size had estimated to be about 20 nm.

Fourier Transform Infrared Spectroscopy (FTIR) spectra of samples showed two distinct absorption bands, the band at $\sim 617(\text{cm}^{-1})$ and the $\sim 426 (\text{cm}^{-1})$ attributed to the tetrahedral and octahedral site respectively. The absorption bands of the tetrahedral site slightly shifted towards high frequency with increasing zinc content.

According to a magnetic measurement, the study indicated that the size of particles was sufficiently small to behave superparamagnetically, the hysteresis loop curves perfectly matched, that evidence the formation of typical soft magnetic materials.

The heating efficiency of water-based ferrofluid studied under magnetic field strength 6.5kA/m and the frequency 190 kHz. The results showed that the heating rate of ferrofluid samples (x=0.3, 0.4 and 0.5) was not changed. Also, constancy of temperature at 44°C when x=0.1 made it favoring for hyperthermia treatment as self-regulate magnetic nanoparticles. Depending on

the increase in the heating curve, the susceptibility, effective relaxation time and Néel relaxation time were determined.

The second series of nanocrystalline $\text{Fe}_{1-x}^{2+}\text{Zn}_x^{2+}\text{Fe}_2^{3+}\text{O}_4^{2-}$ (where $x = 0.0, 0.1, 0.3, 0.5, 0.7, 0.9$ and 1.0) powder has been synthesized by co-precipitation method followed by heat treatment in an autoclave reactor. Identifying and structural characterization of samples had been carried out by using X-ray diffraction. The results demonstrated that all the samples have spinel structure and the zinc ions are engaged within spinel structure. As well as, it is revealed that the pure single phase has been obtained. FE-SEM images had revealed that all samples have homogeneous spherical shape with narrow distribution of the particles size ($\sim 20\text{nm}$). FTIR spectra of $\text{Fe}_{1-x}^{2+}\text{Zn}_x^{2+}\text{Fe}_2^{3+}\text{O}_4^{2-}$ samples showed two distinctive absorption bands lie in the region ~ 561 and $\sim 376\text{ cm}^{-1}$, which indicates formation of spinel structure for ferrite.

Magnetic measurements were performed at room temperature by VSM on both types of samples; condensed nanoparticle (bulk) and nanoparticles that dispersed in paraffin wax. Both types of samples showed negligible coercivity and remanent magnetization. As it revealed the presence of unblocked superparamagnetic nanoparticles in the samples at defined temperature. A significant variation of saturation magnetization was noticed by changing the zinc content in the structure, and highest value has gained at $x=0.5$. Then saturation magnetization gradually decreased with the increase in zinc content.

Heating efficiency of water based ferrofluid samples carried out through hyperthermia experiments. It tested under an alternating magnetic field 6.5 kA/m and frequency 270 KHz , the results showed that the intrinsic loss power (ILP) had doubled at $x=0.3$ as compared with magnetite.

Contents

Subject	Page No.
Table of Contents	I
List of Figures	V
List of Tables	X
List of Symbols	XI
List of Abbreviations	XIV

Table of Contents

Item No.	Subject	Page No.
Chapter One Introduction and Literature Review		1
1.1	Introduction	1
1.2	Literature Review	2
1.3	Aims and Objectives	10
Chapter Two Theoretical and Basic Concepts		11
2.1	Introduction	11
2.2	Origin of Magnetism	11
2.3	Types of Magnetic Materials	13
2.3.1	Diamagnetism	14

2.3.2	Paramagnetism	15
2.3.3	Ferromagnetism	17
2. 3.4	Antiferromagnetism	18
2.3.5	Ferrimagnetism	19
2.4	Crystal Structure of Spinel Ferrite	21
2.4.1	Oxygen positional parameter	23
2.4.2	Theoretical Lattice Parameter	25
2.4.3	Hoping Lengths	26
2.4.4	Bond Lengths	26
2.5	Origin of the Interactions in Ferrimagnetics	27
2.5.1	Direct Exchange Interaction	27
2.5.2	Superexchange Interaction	28
2.6	Hysteresis loop and magnetic parameters	30
2.7	Magnetic Single-Domain	33
2.8	Magnetic Anisotropy	34
2.9	Superparamagnetism	34
2.10	Magnetic Fluid Hyperthermia (MFH)	38
2.11	Theoretical Models and Heat Generation Mechanisms	39
2.12	Magnetic Susceptibility	40
2.13	Magnetization Theory for Ferrofluid	42
2.14	Magnetic Dipolar Interaction	44
2.15	Brownian Relaxation	45
2.16	Neel Relaxation	46
2.17	Effective Relaxation	47
2.18	Specific Absorption Rate (SAR) or Specific Loss Power (SLP)	47

2.18.1	Corrected Slope Method	50
2.18.2	Box–Lucas method	51
2.19	Induction Heater	51
2.20	Magnetic Nanoparticles in Biomedical Applications	52
2.20.1	Magnetic Separation	52
2.20.2	Magnetic Resonance Imaging (MRI)	53
2.20.3	Drug Delivery	53
2.20.4	Cancer	54
2.20.5	Hyperthermia	55
2.21	Nanofluids	56
2.21.1	Specific Heat of Nanofluid	57
2.21.2	Specific Heat Models	58
2.22	Specific Heat Capacity	59
2.23	Stabilisation of Nanoparticles	59
2.23.1	Electrostatic Stabilization	59
2.23.2	Steric Stabilization	60
2.24	Synthesis of Ferrite Nanoparticles	61
2.24.1	Co- Precipitation	61
2.24.2	Hydrothermal/solvothermal Methods	62
2.25	Characterization of MnZn-Ferrite	62
2.26	Characterization of $\text{Fe}_{1-x}^{2+}\text{Zn}_x^{2+}\text{Fe}_2^{3+}\text{O}_4^{2-}$ ferrites	63
2.27	X-ray Diffraction (XRD)	64
2.28	Fourier Transform Infrared (FTIR) spectroscopy	67
Chapter Three Experimental Part		68
3.1	Introduction	68

3.2	Materials and Method	68
3.2.1	Raw Materials and Chemicals	68
3.2.2	Synthesis of Ferrite Nanoparticles	71
3.2.3	Preparation of Ferrofluid Samples	74
3.3	Structural Characterization	75
3.3.1	X-ray Diffraction (XRD)	75
3.3.2	Fourier Transform Infrared Spectroscopy (FT-IR).	75
3.3.3	FE-SEM Image Analysis	75
3.4	Magnetic Properties	76
3.4.1	Vibrating Sample Magnetometer (VSM)	76
3.5	Differential Scanning Calorimetry (DSC)	77
3.6	Heating Efficiency	77
3.7	Effective Relaxation Time and Néel Relaxation Time Calculations	78
Chapter Four Results and Discussion		80
4.1	Introduction	80
4A.1	Structural Properties of $Mn_{1-x}Zn_xFe_2O_4$ nanoparticles	81
4A.1.1	XRD Analyses	81
4A.1.2	FTIR Spectroscopy Analysis	88
4A.1.3	FESEM image analysis	92
4A.2	Magnetic Properties	96
4A.3	Heating Efficiency	99
4A.3.1	Specific Heat of $Mn_{1-x}Zn_xFe_2O_4$ Nanofluids	100
4A.3.2	Heat Dissipation Mechanisms	101
4B.1	Structural Properties of $Fe_{1-x}^{2+}Zn_x^{2+}Fe_2^{3+}O_4^{2-}$ Nanoparticles	103

4B.1.1	XRD Analyses	103
4B.1.2	FT-IR spectroscopy analysis	107
4B.1.3	FE-SEM Image Analysis	110
4B.2	Magnetic Properties	112
4B.3	Superparamagnetic properties of $\text{Fe}_{1-x}^{2+}\text{Zn}_x^{2+}\text{Fe}_2^{3+}\text{O}_4^{2-}$ nanoparticles	116
4B.3.1	Comparison between domain magnetization (M_d) and bulk magnetization (M_B) of $\text{Fe}_{1-x}^{2+}\text{Zn}_x^{2+}\text{Fe}_2^{3+}\text{O}_4^{2-}$ samples	119
4B.4	Heating efficiency of $\text{Fe}_{1-x}^{2+}\text{Zn}_x^{2+}\text{Fe}_2^{3+}\text{O}_4^{2-}$ nanoparticles	123
4B.4.1	Specific Heat of nanofluids	125
4.2	Conclusions	126
4.3	Suggestions for Future Work	127
References		128
Appendix		148

List of Figures

Fig. No.	Figure Caption	Page No.
2.1	Periodic table showing different kinds of magnetic materials	14
2.2	(a) Diamagnetic material: The atoms do not possess magnetic moment,.....	15
2.3	(a) Paramagnetic material: Each atom possesses a permanent magnetic moment,.....	17
2.4	Ferromagnetism	18
2.5	Antiferromagnetism	19
2.6	Ferrimagnetism	20

2.7	Unit cell of spinel structure MeFe_2O_4	21
2.8	Normal spinel ferrites	22
2.9	Inverse spinel ferrites	23
2.10	Mixed spinel ferrites	23
2.11	Slater-Bethe curve showing the magnitude and sign of the exchange integral as a function of D/d	28
2.12	Super-exchange Interactions	29
2.13	Hysteresis loop for ferromagnetic materials	31
2.14	Variation of the coercive field with nanoparticle size	35
2.15	The energy density of a magnetic particle contains a term $K\sin^2\theta$, the energy is minimized when $\theta = 0$ or π .	36
2.16	The dependence of the relaxation time (τ) as a function of temperature T (scaled by k_B/KV),.....	37
2.17	The normalized χ' and χ'' as functions of $\omega\tau$, the out-of-phase component χ'' reaches a maximum when $\omega\tau=1$.	41
2.18	The theoretical Langevin equation (2.23) is plotted with low and high-field asymptotes (dashed lines)	43
2.19	Comparison of Neel (A) and Brown (B) relaxations	45
2.20	Typical heating curves obtained in calorimetric measurements with an adiabatic and a non-adiabatic setup.	49
2.21	The numerical derivatives of a cooling curve versus the temperature difference after heating of sample.	50
2.22	Influence of heating on blood vessels in healthy tissue (above) versus tumour tissue with pathologic vessels (below)	55
2.23	A representation of stabilization of nanoparticles with (a)	61

	charge and (b) steric methods	
2.24	Schematic representation of x-ray diffraction	65
2.25	Constructive interference from the parallel planes	65
3.1	Preparation steps of ferrite nanoparticles by co-precipitation method.	71
3.2	Hydrothermal autoclave reactor	72
3.3	Flow chart of co-precipitation method followed by heat treatment in an autoclave reactor	73
3.4	Synthetic ferrofluid samples	74
3.5	Heating system	78
4.1	XRD patterns of the synthesized $Mn_{1-x}Zn_xFe_2O_4$ nanoparticles and the phase composition of prepared samples by co-precipitation method	82
4.2	XRD patterns of the synthesized $Mn_{1-x}Zn_xFe_2O_4$ nanoparticles and the phase composition of the samples that have thermally treated in an autoclave reactor.	83
4.3	Variation of theoretical and experimental lattice constant for $Mn_{1-x}Zn_xFe_2O_4$ as a function of Zn^{2+} content	85
4.4a	FTIR spectrum of $Mn_{1-x}Zn_xFe_2O_4$ samples	89
4.4b	Identifying and analyzing the characteristics of the FTIR absorbance band for $Mn_{1-x}Zn_xFe_2O_4$ samples (magnified view)	90
(4.5a)	FESEM image of samples that have been obtained by co-precipitation method in the left and the images after heat treatment by hydrothermal autoclave reactor in the right (samples $x=0, 0.1$ and 0.2)	93
4.5b	FESEM image of samples that have been obtained by co-	94

	precipitation method in the left and the images after heat treatment by hydrothermal autoclave reactor in the right (samples $x=0.3, 0.4$ and 0.5).	
4.5c	Histograms showing the particle size distributions of $Mn_{1-x}Zn_xFe_2O_4$ nanoparticles,.....	95
4.6a	Magnetization versus applied magnetic field of $Mn_{1-x}Zn_xFe_2O_4$ nanoparticles at 300K	97
4.6b	The magnified view of hysteresis loop at low field	97
4.6c	Fitting of magnetization curves M near about saturation magnetization as a function of inverse-square magnetic field at range 3.6-8 kOe	98
4.7	Heating curves for $Mn_{1-x}Zn_xFe_2O_4$ ferrofluids under alternate magnetic field strength 6.5KA/m and frequency 190 KHz	100
4.8	Specific heat capacity for $Mn_{1-x}Zn_xFe_2O_4$ nanoparticles as a function of temperature	101
4.9	XRD patterns of the synthesized $Fe_{1-x}Zn_xFe_2O_4$ nanoparticles.	104
4.10	Variation of theoretical and experimental lattice constant for $Fe_{1-x}^{2+}Zn_x^{2+}Fe_2^{3+}O_4^{2-}$ as a function of Zn^{2+} content	105
4.11	FTIR spectra of $Fe_{1-x}^{2+}Zn_x^{2+}Fe_2^{3+}O_4^{2-}$ samples.	108
4.12a	A series of FE-SEM images for $Fe_{1-x}^{2+}Zn_x^{2+}Fe_2^{3+}O_4^{2-}$ nanoparticles (Samples $x=0, 0.1, 0.3$ and 0.5).	110
4.12b	A series of FE-SEM images for $Fe_{1-x}^{2+}Zn_x^{2+}Fe_2^{3+}O_4^{2-}$ nanoparticles (Samples $x=0.7, 0.9$ and 1)	111
4.12c	Histograms showing the particle size distributions of $Fe_{1-x}^{2+}Zn_x^{2+}Fe_2^{3+}O_4^{2-}$ nanoparticles.	112
4.13A	Magnetization curves of $Fe_{1-x}^{2+}Zn_x^{2+}Fe_2^{3+}O_4^{2-}$ condensed	113

	nanoparticles at room temperature (300K).	
4.13B	Shows the magnified view of hysteresis loop	114
4.13C	Fitting of magnetization curves M near about saturation magnetization as a function of inverse-square magnetic field at range (3-6) KOe.	114
4.14	Variation of saturation magnetization for $\text{Fe}_{1-x}^{2+}\text{Zn}_x^{2+}\text{Fe}_2^{3+}\text{O}_4^{2-}$ nanoparticles as a function of zinc content (x).	115
4.15A	Magnetization curves of $\text{Fe}_{1-x}^{2+}\text{Zn}_x^{2+}\text{Fe}_2^{3+}\text{O}_4^{2-}$ superparamagnetic nanoparticles for at room temperature (300K)	117
4.15B	The magnified view of hysteresis loop for $\text{Fe}_{1-x}^{2+}\text{Zn}_x^{2+}\text{Fe}_2^{3+}\text{O}_4^{2-}$ samples.	118
4.15C	Fitting of magnetization curves M near about saturation magnetization as a function of inverse-square magnetic field at range (3-6) KOe.	118
4.16	Ratio of the thermal energy to the magnetic dipolar interaction energy at a distance 165nm for $\text{Fe}_{1-x}^{2+}\text{Zn}_x^{2+}\text{Fe}_2^{3+}\text{O}_4^{2-}$ superparamagnetic nanoparticles.	121
4.17	Comparative data for domain magnetization of a series $\text{Fe}_{1-x}^{2+}\text{Zn}_x^{2+}\text{Fe}_2^{3+}\text{O}_4^{2-}$ superparamagnetic nanoparticle (Md) versus magnetization of condensed nanoparticles (bulk) at room temperature.	122
4.18	Heating curves for $\text{Fe}_{1-x}^{2+}\text{Zn}_x^{2+}\text{Fe}_2^{3+}\text{O}_4^{2-}$ ferrofluids under alternate magnetic field strength 6.5KA/m and frequency 270 KHz.	124

4.19	Variation of the ILP values as a function of Zn content for the $\text{Fe}_{1-x}^{2+}\text{Zn}_x^{2+}\text{Fe}_2^{3+}\text{O}_4^{2-}$ samples.	125
------	--	-----

List of Tables

Table No.	Table caption	Page No.
2.1	Interatomic distances and site radii in spinel structure (AB_2O_4) as a function of unit cell edge (a) and deformation parameter (u).	24
2.2	Ionic radii of various cations (in Å)	26
3.1	List of chemical compounds that are used in the current study	69
3.2	Synthesis of $\text{Mn}_{1-x}^{2+}\text{Zn}_x^{2+}\text{Fe}_2^{3+}\text{O}_4^{2-}$ from basic chemicals compounds and the weights that had been used	70
3.3	Synthesis of $\text{Fe}_{1-x}^{2+}\text{Zn}_x^{2+}\text{Fe}_2^{3+}\text{O}_4^{2-}$ from basic chemicals compounds and the weights that had been used	70
4.1	Crystallographic parameters for $\text{Mn}_{1-x}\text{Zn}_x\text{Fe}_2\text{O}_4$ nanoparticles	88
4.2	IR absorption bands and force constants of the $\text{Mn}_{1-x}\text{Zn}_x\text{Fe}_2\text{O}_4$ samples	91
4.3	The variation of magnetic parameters for $\text{Mn}_{1-x}\text{Zn}_x\text{Fe}_2\text{O}_4$ nanoparticles as a function of the zinc content	98

4.4	Heating efficiency parameters of ferrofluid samples for $Mn_{1-x}Zn_xFe_2O_4$.	101
4.5	Superparamagnetic parameters of ferrofluid samples $x=0, 0.1$ and 0.2 , which had generated heat under the alternating magnetic field $H=6.5$ kA/m and $f=190$ kHz.	102
4.6	Crystallographic parameters for $Fe_{1-x}^{2+}Zn_x^{2+}Fe_2^{3+}O_4^{2-}$ nanoparticles.	107
4.7	IR absorption bands and force constants of the $Fe_{1-x}^{2+}Zn_x^{2+}Fe_2^{3+}O_4^{2-}$ samples.	109
4.8	Variation of magnetic parameters of condensed nanoparticles for $Fe_{1-x}^{2+}Zn_x^{2+}Fe_2^{3+}O_4^{2-}$ samples.	116
4.9	Variation of magnetic parameters of superparamagnetic nanoparticles for $Fe_{1-x}^{2+}Zn_x^{2+}Fe_2^{3+}O_4^{2-}$.	119
4.10	Superparamagnetic properties of $Fe_{1-x}^{2+}Zn_x^{2+}Fe_2^{3+}O_4^{2-}$ samples	122
4.11	Heating efficiency parameters of $Fe_{1-x}^{2+}Zn_x^{2+}Fe_2^{3+}O_4^{2-}$ ferrofluids	123

List of Symbols

Symbol	Meaning	Units
f	Frequency	Hz

H	Magnetic field amplitude	A/m
SAR	Specific absorption rate	W/g
SLP	Specific loss power	W/g
ILP	Intrinsic loss power	$\text{nHm}^2 \text{kg}^{-1}$
μ_0	Permeability of free space	$4\pi \times 10^{-7} \text{Hm}^{-1}$
μ_r	Relative permeability	Dimensionless
μ	Magnetic permeability of the medium	Hm^{-1}
T_N	Néel temperature	K or °C
Tc	Curie temperature	K or °C
u	Oxygen positional parameter	--
a_{th}	Theoretical lattice constant	Å
L	Hopping length	Å
$d_{\text{A-O}}$	Tetrahedral bond length	Å
$d_{\text{B-O}}$	Octahedral bond length	Å
Ms	Saturation magnetization	emu/g
Bs	Saturation flux density	Tesla (T)
Br	Remnant induction	Tesla (T)
Hc	Magnetic coercivity	A/m
μ_1	Magnetic moment	$\text{A}\cdot\text{m}^2$
K_u	Uniaxial anisotropy constant	Jm^{-3}
τ_0	Characteristic relaxation time	s
τ_N	Néel relaxation time	s
τ_B	Brown relaxation time	s
τ	Effective relaxation time	s
T_B	Blocking temperature	K

χ	Magnetic Susceptibility	--
χ'	Real part of Magnetic Susceptibility	--
χ''	Imagery part of Magnetic Susceptibility	--
χ_0	Initial Susceptibility	--
M_d	Domain magnetization	emu/g
k_B	Boltzmann's constant	$1.38 \times 10^{-23} \text{ J}\cdot\text{K}^{-1}$
T	Absolute temperature	K
$C_{P,nf}$	Specific heat of nanofluid	J/g. $^{\circ}$ C
h, k, l	Miller indices	--
ρ_x	X-ray density	g/cm ³
D	Crystallite size	nm
N_A	Avogadro's number	6.023×10^{23} (atom/mole)
λ	Wavelength	nm
amu	Atomic Mass Unit	$1.661 \times 10^{-24} \text{ g}$
f_r	Resonance frequency	Hz
N	Number of turns	Integer
I	Current	Ampere (A)
a_{exp}	Experimental lattice constant	Å
ν	Wavenumber	cm ⁻¹
M_r	Remnant magnetization	emu/g
$\frac{\Delta T}{\Delta t}$	Heating rate	K/s
C_p	Specific heat	J/g. $^{\circ}$ C.
K	Magneto-crystalline anisotropy constant	Jm ⁻³

E_{Th}	Thermal energy	Joule
E_{dd}	Dipole - dipole interaction energy	Joule

List of Abbreviations

Abbreviation	Definition
MNPs	Magnetic nanoparticles
MFH	Magnetic fluid hyperthermia
FI	Faceted Irregular
NPs	Nanoparticles
AMF	Alternating Magnetic Field
CZF	Cobalt-Zinc Ferrite
DDW	Double Distilled Water
DLS	Dynamic Light Scattering
fcc	Face center cubic
FI	Faceted Irregular
FM	Ferromagnetic Material
MFH	Magnetic Fluid Hyperthermia
M-H	Magnetization versus applied magnetic field
MNPs	Magnetic nanoparticles
MRI	Magnetic Resonance Imaging
PEG	Polyethylene glycol
SQUID	Superconducting Quantum Interference Device
TEM	Transmission Electron Microscopy
XRD	X-Ray Diffraction

FTIR	Fourier Transform Infrared Spectroscopy
FESEM	Field Emission Scanning Electron Microscopes
VSM	Vibrating Sample Magnetometer
DSC	Differential Scanning Calorimetry
KBr	Potassium Bromide
JCPDS	Joint Committee on Powder Diffraction Standards
LAS	Law of Approach to Saturation
LCR circuit	Is an electrical circuit consisting of a resistor (R), an inductor (L), and a capacitor (C).

Chapter One

Introduction and Literature Review

1.1 Introduction

Nanotechnology deals with small structures or small-sized materials. The typical dimension spans from sub-nanometer to several hundred nanometers. A nanometer (nm) is one billionth of a meter, or 10^{-9} m. Materials in the nanometer scale may exhibit physical properties distinctively different from that of bulk. In the United States, nanotechnology has been defined as being “concerned with materials and systems whose structures and components exhibit novel and significantly improved physical, chemical and biological properties, phenomena and processes due to their nanoscale size [1].

Magnetic nanoparticles (MNPs) are one of the most important categories of nano-materials which are magnetically unique. The most important features magnetic nanoparticles are; high field irreversibility, high saturation region, Superparamagnetism, extra anisotropy and temperature-dependended hysteresis, etc [2].

The magnetic nanoparticles for bio-applications have piqued interest to researchers due to their close dimensions to the biological entities and special magnetic properties. Despite the fact that most living organisms are consisting of cells that are around 10 μm in size, the cell's dimensions are frequently much smaller, typically in the nanoscale. For examples the dimensions of genes are 10–100 nm in length and 2 nm in width, proteins ranged in size from 5 to 50 nm, while viruses were 20 to 450 nanometers [3].

The dimensions of synthetic magnetic nanoparticles can be regulated, and nanoparticles as small as a few nanometers in diameter can be synthesized

using specifically designed experimental procedures and carefully controlled reaction conditions. With the advent of nanoscale the magnetic nanoparticle became an interest, especially as its dimensions get close or smaller than biological entities [4].

Furthermore, covering nanoparticle with biomaterials prevents the interaction between nanoparticle and biological entities in addition to enhancing their suitability for biomedical applications, a process known as bio-functionalization. It allows a more precise method of 'tagging' or resolving nano-scale linking. Magnetic nanoparticles had been used as really quite sensitive sensors to observe physiological systems at the cellular scale without interfering with them. In fact, because of their noninvasive nature, magnetic and optical effects have been regarded as the most effective methods for biological applications [5].

Magnetic nanoparticles (MNPs) generate heat when exposed to an alternating magnetic field. As a result, MNPs are used in the treatment of cancer with magnetic fluid hyperthermia (MFH), and have been shown to increase the efficacy of chemotherapy and/or radiation treatment in clinical trials. Owing to inadequate MNPs, uneven distribution of MNPs in the tumor, or heat loss to the nearby region, current MFH treatment was unable to provide adequate heat to the tumor [6].

1.2 Literature Review

Magnetic nanoparticles are widely used in biomedical applications. The benefit of this kind of nanoparticle is that, it can be controlled by a magnetic field. So it can be used as a drug delivery and, magnetic resonance imaging (MRI) contrast. Magnetic nanoparticles produce heat when subjected

to an alternating magnetic field; as a result, they are used in hyperthermia. Ferrofluid consist from the dissipation of magnetic nanoparticles in suitable carrier liquid, which should be stabilized in a liquid using the proper surfactant [7].

Many researchers worked on different types of magnetic nanoparticles to study the physical properties; shape and size of nanoparticles, crystal structure, and heat released. The following are a few notable works that dealt with concern of the thesis:

Fortin et al. (2007) synthesized maghemite and cobalt ferrite nanoparticles of various sizes ranged from 5 to 20 nm dispersed in water and other solvent formed from water and glycerol with various viscosities they attempted to differentiate between the Néel and Brown contributions in the energy production. Specific absorption rate (SAR) values of cobalt ferrite and maghemite samples were measured under alternating magnetic field with frequency ($f = 700$ kHz) and amplitude ($H = 24.8$ kA.m⁻¹). They attributed higher SAR values to Brownian friction in cobalt ferrite while Néel relaxation mechanism in maghemite nanoparticles led to higher SAR values. The SAR values ranged from 4 to 1650 W/g with increasing particle size of maghemite from 5.4nm to 16.5nm [8].

Pradhan et al. (2007) studied on a series of superparamagnetic nanoparticles of magnetite, manganese and cobalt ferrites. Nanoparticles were coated with lauric acid and assessed their thermal efficiency and biocompatibility to test whether they could be used in cancer hyperthermia therapy. The particles in all of the magnetic fluids were 9–11 nm in size on average. The calorimetric measurements of SAR values was assessed at frequency 300 kHz and field 15 kA/m to investigate the heating efficiency of magnetic fluids. They found that

the SAR values were higher in magnetite (120 W/g) and manganese ferrite (97 W/g) than in cobalt ferrite 37 W/g [9].

Joshi et al. (2009) synthesized the cobalt ferrite magnetic nanostructures via seeded growth thermal decomposition. Seed mediated growth of nanocrystals in the organic phase was used to create spherical nanostructures of different sizes, whereas faceted irregular (FI) CoFe_2O_4 nanostructures were produced using the similar procedure but, under applied magnetic field and nanoparticles dispersed in water. The study found that the spherical nanoparticle is superior to faceted irregular equivalents in saturation magnetization (M_s), as well as the magnitude of M_s increased with size. SAR experiments were made with RF generator at a power of 5 kW and frequency of 300 kHz. The specific absorption rate (SAR) of nanostructures has been observed to increase with increasing size, while cobalt ferrite (FI) showed less saturation magnetization and low SAR value than spherical nanostructures [10].

Suto et al. (2009) used the coprecipitation method to prepare magnetite samples A and B; A sample had a diameter of 12.5 nm, while B had a diameter of 15.7 nm. Both Néel and Brownian relaxations were essential for the particles in heating process. A second collection of samples was made using a polyvinyl alcohol hydro-gel to disperse equal solid concentrations. The magnetic moment was only relaxed by Néel relaxation for the dispersed samples in the gel because nanoparticle motion was limited. SAR calculations were recorded at frequency 600 kHz with amplitude of 40 Oe. They discovered that heating mechanisms were dependent on particle dispersion states, and that specific absorption rates decreased as the viscosity of the medium increased due to reduced Brownian relaxation contributions [11].

Alphandéry et al. (2011) studied on the magnetotactic bacterium *Magnetospirillum magneticum* strain AMB-1 when it is subject to the same magnetic field, the researchers investigated the mechanisms of heat generation by entire cells and individual magnetosomes. The individual magnetosomes showed higher SAR values compared to intact cells. The higher SAR values are attributed due to rotation of magnetosomes nanoparticles in the magnetic field [12].

Hugounenq et al. (2012) developed innovative nanostructures for high efficiency magnetic hyperthermia exceed of the superparamagnetic size range. When the synthesis was performed in a combination of N-methyldiethanolamine and diethylene glycol, the alkaline hydrolysis of iron (III) and iron (II) chlorides produced nanoparticles with flowerlike shape. Under such experimental circumstances, flowerlike nanostructure was caused by the arrangement of nanoparticles having sizes about 11 nm. The propagation technique allows for modulation of the nanoflower's size, magnetic properties and polycrystalline character, resulting in a significant increase in their heat, with the highest value $SLP = 1944\text{W/g}$ for flower-like maghemite nanoparticles with a diameter of 28nm. It studied under an alternating magnetic field with frequency 700 kHz and an amplitude 21.5 kA/m [13].

Guardia et al. (2012) investigated the hyperthermia properties of cube-shaped iron oxide nanocrystal samples prepared by thermal decomposition in various sizes (12, 19, 25, 38) nm, with regular-shaped nanocubes acquired at 19,25nm. The SAR values for the different iron oxide nanocrystal sizes studied at different frequencies and magnetic field amplitudes showed that 19 nm sample performed the best under all experimental conditions. At 520 kHz

and 29 kAm^{-1} , SAR values achieved $2452 \text{ W/g}_{\text{Fe}}$, that is one of the maximum power ever recorded for iron oxide nanoparticles. In vitro tests on KB cancer cells treated with 19 nm iron oxide nanocrystals (IONCs) revealed effective hyperthermia results. After an hour of hyperthermia treatment at a temperature $43 \text{ }^\circ\text{C}$, cell mortality was about 50% [14].

Veverka et al. (2014) used the co-precipitation method to make magnetic cores of $\text{Co}_{0.4}\text{Zn}_{0.6}\text{Fe}_2\text{O}_4$ of two different sizes, which were annealed at temperatures of $500 \text{ }^\circ\text{C}$ and $650 \text{ }^\circ\text{C}$. The nanoparticles were encapsulated in silica, which resulted in colloidally stable water suspensions. The increase of annealing temperatures had caused a significant rise in Curie temperatures (T_c) and blocking temperature (T_B), additionally the heating efficiency of sample had been enhanced [15].

Blanco et al. (2015) synthesized citric acid coated iron oxide magnetic nanoparticles with the benefit of microwave and provided an effective, controllable, and easily scalable method to manufacture multi-core structures for magnetic hyperthermia purposes. A decreasing hydrodynamic diameter had occurred as the concentration of citrate ions in solution increases (D_H). The core radius and the overall hydrodynamic width of the multi-core particle have been considered to be significant structural factors in magnetic heating efficiency. Large cores in small ensembles ($D_H = 65 \text{ nm}$) produced the best results [16].

Fantechi et al. (2015) synthesized $\text{Co}_x\text{Fe}_{3-x}\text{O}_4$ nanoparticles with an 8 nm size using a thermal decomposition method. They noticed that the increase in concentration of Cobalt would significantly increase the SAR values. The SAR goes up with x, and it peaks at $x=0.6$. The intrinsic magnetic properties,

especially the magnetic anisotropy were thought to be responsible for this behavior [17].

Aneja et al. (2017) used a hydrothermal process to synthesize superparamagnetic $\text{La}_{0.77}\text{Sr}_{0.23}\text{MnO}_3$ nanoparticles with diameter of 18 nm. The pseudo-cubic perovskite crystalline nature was confirmed by structural analysis. The superparamagnetic behavior of the prepared particles was revealed by M-H hysteresis curve. Various concentrations of distilled water (2–20 mg/mL) were used. They found that the hyperthermia temperature 42–43°C can be reached with a concentration less than 3 mg/mL under experimental conditions (frequency of 267 kHz and an amplitude 293.3 and 335.3 Oe) [18].

Srivastava et al. (2018) used quite stable, quick, and one-step microwave refluxing method to synthesize $\text{Zn}_x\text{Fe}_{3-x}\text{O}_4$ spinel type structure, where x varied from 0.01 to 0.8. TEM analysis revealed that the particles were between 3 and 11 nm in size. Ferrofluid samples were prepared by dissolved magnetic nanoparticles in different carrier medium; water (4mL) and oleic acid (8 mL). For 20 minutes at 60°C, this solution was continuously stirred. Every ferrofluid had a 42 mg/mL MNPs concentration. For the sample with x = 0.2, the maximum SAR value was recorded at frequency 478 kHz with field strength 11 mT. The higher SAR value was attributed to higher Ms value [19].

Mello et al. (2019) reported the synthesis of $\text{Zn}_x\text{Mn}_{0.4-x}\text{Fe}_{0.6}\text{Fe}_2\text{O}_4$; where x changed from 0 to 0.4 using the co-precipitation process, and the existence of poly ethylene glycol (PEG) at 353K. The presence of PEG ensures the size of the nanoparticles ranging from 10 to 15 nanometers. Hyperthermia measurement had performed on ferrofluid samples with concentration 10

mg/ml in a citric acid solution with a pH of 5. Additionally the experiment carried out at magnetic field strength 25 mT and frequency 112 kHz. The results showed Zn additions decreased the hyperthermia efficiency, as well as the magnetic hyperthermia factor had been attributed primarily to the Néel-Brownian relaxation mechanism [20].

Shaw et al. (2019) had used microwave-assisted polyol process to create magnetic nano-flowers with the mean diameter of 50nm and a blend of seed (MnFe_2O_4) and soft magnetic phases ($\gamma\text{-Fe}_2\text{O}_3$). The nano flowers outperformed MnFe_2O_4 single cores in terms of heating efficiency and magnetic properties. Nanoflowers had a three-fold higher ILP value ($3.30 \text{ nHm}^2 \text{ Kg}^{-1}$) than single core MNPs when subjected to an alternating magnetic field with a frequency of 113 kHz and amplitude of 250 Oe. The ILP obtained value was higher than that of magnetic colloids marketed commercially. The HeLa cells were killed significantly by the hyperthermia treatment with a concentration of 0.75 mg/mL for 30 minutes, and their viability was reduced by up to 17% [21].

Dhumal et al. (2019) prepared citric acid coated nanoferrites having composition $\text{Fe}_{1-x}\text{Mn}_x\text{Fe}_2\text{O}_4$ ($x = 0.0, 0.1, 0.3, 0.5, 0.7, 0.9$ and 1.0) by chemical co-precipitation method. Samples (5 mg/ml of distilled water) were put in the coil's middle, with a frequency of 289 kHz and changing amplitudes of field to 167.6, 251.4 and 335.2 Oe. The SAR varies in a similar manner to saturation magnetization (Ms). SAR reached a maximum (100W/g under field amplitude 335.2 Oe) when $x=0.7$ it is observed that the value increased by 20% in $\text{Fe}_{0.3}\text{Mn}_{0.7}\text{Fe}_2\text{O}_4$ as compared to Fe_3O_4 [22].

Kowalik et al. (2020) prepared yttrium-doped of magnetite by a co-precipitation method by variable percentage of Y^{3+} (0, 0.1, 1, and 10%) ions.

The experiments had been made to increase the heating abilities for magnetic hyperthermia. The excellent results were obtained for the ILP values which equals $1.85 \text{ nHm}^2/\text{kg}$ at 0.1% Y^{3+} ions doping in Fe_3O_4 [23].

Gu et al. (2020) studied two types of magnetic nanoparticles; $\epsilon\text{-Fe}_2\text{O}_3$ and $\gamma\text{-Fe}_2\text{O}_3$ with similar size of the same size (20 nm). The heating efficiency of uncoated and polymer-coated samples was measured over a broad range of field amplitude and frequency. In medium with a viscosity comparable to that of cell cytoplasm, $\epsilon\text{-Fe}_2\text{O}_3$ nanoparticles were observed to heat primarily in the low-frequency range (20–100 kHz). At high frequency range (400–900 kHz), on the other hand, $\gamma\text{-Fe}_2\text{O}_3$ nanoparticles heat more effectively [24].

Rajan et al. (2020) conducted an investigation on magnetite (Fe_3O_4) nanoparticles coated with various surfactants such as cetyl-trimethyl ammonium bromide (CTAB), citric acid (CA), ethylene diamine (EDA), polyvinylpyrrolidone (PVP), polyethylene glycol (PEG), and glutamic acid (GA). It is prepared by using the co-precipitation process, and their inductive heating efficiency for hyperthermia applications is compared. The results showed that there is considerable discrepancy in magnetic anisotropy, magnetic susceptibility and magnetic relaxation time. As a result, these findings open up a lot of possibilities for developing surface coated magnetite NPs for hyperthermia applications [25].

Manohara et al. (2020) synthesized of CoFe_2O_4 nanoparticles using the solvo-thermal reflux method. Under biocompatible alternative magnetic field limitations, the peculiarity of magnetic hyperthermia in cobalt-ferrite was tested. Heating ability's of magnetic ferrofluid for CoFe_2O_4 at concentration 3 mg/mL can be reached up to 185.32 W g^{-1} , this count was greater than those

of other SAR that recorded by other methods for synthesized CoFe_2O_4 nanoparticles [26].

1.3 Aims and Objectives

- Synthesis of $\text{Mn}_{1-x}\text{Zn}_x \text{Fe}_2\text{O}_4$ nanoparticles where $x=0-0.5$ with a step of 0.1 by using a co-precipitation method and, study the effect of zinc replacement on the structural properties, magnetic properties, and heating efficiency of ferrofluid samples.
- Studying the influence of zinc replacement in magnetite structure on the structural properties, magnetic properties, and the heating efficiency of magnetite for hyperthermia through synthesis of $\text{Fe}_{1-x}^{2+}\text{Zn}_x^{2+}\text{Fe}_2^{3+}\text{O}_4^{2-}$ nanoparticles where $x = 0.0, 0.1, 0.3, 0.5, 0.7, 0.9,$ and 1.0 .